Hydrothermic Reduction of Rutile-Ilmenite Mineral Producing an Oxyhydride η-$Ti_2FeO_{0.2}H_{2.8}$: Towards In-Situ Hydrogen Production and Storage

I. A. Mohammed[1], S. I. Mustapha[1*], F. A. Aderibigbe[1], H. U. Hambali[1], A. M. Afolabi[1], K. B. Muritala[1], U. M. Aliyu [2]

[1]Department of Chemical Engineering, University of Ilorin, P.M.B. 1515, Ilorin, Nigeria
[2]Department of Chemical Engineering, Abubakar Tafawa Balewa University, Bauchi, Nigeria

ABSTRACT: As an alternative to the physical storage of hydrogen as compressed gas or liquid hydrogen requiring high-pressure tanks and cryogenic temperatures, the material-based storage of hydrogen in solids involves hydrogen uptake and release from the surface of adsorbents or within interstitials of hydrides. We report a hydrothermic reduction of rutile-ilmenite mineral into hydrogen-rich fibrous products, η-$Ti_2FeO_{0.2}H_{2.8}$, in an ethanol-water system at 120°C for 4 hrs. As part of a project to generate hydrogen from water-ethanol system using advanced catalysts containing graphene oxide (GO) as carbon source, a system of 62.5 µg graphene oxide per g of rutile-ilmenite mineral was employed in a concentration of 50 mg/mL of ethanol-water solution. As well as in the original mineral, XRD of thermal annealed mineral between 500 and 800°C showed no hydride or phase change in rutile-ilmenite. With hydrothermal treatment of GO/rutile-ilmenite (50 mg/mL) in ethanol-water (1:1 v/v) at 120°C, a hydrogen-rich ferrotitanium hydride phase was formed, and there was a change in morphology from plate-like and granular particles into fibrous structures. Like the release of hydrogen by its 'carriers' (e.g., CaH_2, NH_4BH_4, $NaBH_4$, NH_3, formic acid), it is anticipated that hydrogen was generated from the ethanol-water system in-situ, which reduced the rutile-ilmenite mineral into a hydride. EDX results showed that the reduction affected specifically the oxides of Fe and aluminosilicates in the mineral. The study demonstrated a possibility of in-situ hydrogen generation and storage via low-temperature graphene oxide hydrothermic reduction of rutile-ilmenite mineral in an ethanol-water system.

KEYWORDS: Hydrogen, hydrothermic, ethanol-water, rutile-ilmenite, graphene oxide

[Received Oct. 31, 2023; Revised Dec. 28, 2023; Accepted Feb 6, 2024] Print ISSN: 0189-9546 | Online ISSN: 2437-2110

I. INTRODUCTION

Several hydrogen storage materials were developed but are either unstable at the required temperature or tend to show low hydrogen carrying capacity. For example, ferrotitanium alloys are well-known hydrogen-storage materials (Ma *et al.*, 2006). Whereas rutile is a stable form of titania that could be a product of anatase irreversible transformation at elevated temperatures (Hanaor and Sorrell, 2011). The hydrothermal reduction of ilmenite or its alloy in alkaline media has been reported in a few studies. Simpraditpan *et al.*, (2013) observed the formation of nanofibers using 72-hr hydrothermal treatment of ilmenite ore in an alkaline solution of 10 M NaOH. Their XRD result showed a hydride of the mineral was formed after the hydrothermal treatment, which was identified as a layered titanate H2TixO2x+1 structure. There was a complete transformation into nanofibers morphology.

In contrast, a study of hydrothermal treatment of rutile-quartz concentrates at 200°C for 1 hr in 5 M NaOH only obtained a partial transformation into fiber-like structures. XRD showed no hydride formation (Zanaveskin *et al.*, 2014). While some studies attribute the formation of amorphous phases or nanofibers to the dissolution of impurities such as ilmenite, silica/quartz, and others (Simpraditpan *et al.*, 2013; Zanaveskin *et al.*, 2014), the selected area EDS in the work of Zanaveskin *et al.*, (2014) indicates that the formed rod-like phases may not be due to ilmenite but to aluminosilicate impurities including some Ti and C in the mineral. Since there are other impurities such as MgO, CaO, ZnO and others in the samples (Simpraditpan *et al.*, 2013), it therefore becomes complicated to identify the specific compound responsible for the reduction of ilmenite-rutile mineral into hydrides.

Reduction of ilmenite can occur in any favourable reducing medium. Taguchi *et al.*, (2020) recently observed the formation of amorphous iron hydrides in aqueous solutions at ambient conditions. The two forms, nanowires and granular, undergo transformation to crystalline α-Fe by heat treatment at 600°C. The nanowire hydride exhibits a hydrogen content of 0.10 wt%, while the granular iron hydride of 0.22 wt%. In their study, an aqueous NaBH4 solution was added to the Fe_{2+} solution and no other chemical was involved. It therefore implies that the chemical hydrides such as $NaBH_4$ can reduce the inorganic soluble species e.g., layered clusters into rod-like morphologies via hydrogenation. However, minerals are complicated for understanding of the specific reducing agents due to the presence of several potential reductants.

*Corresponding author: mustapha.si@unilorin.edu.ng *doi:* http://dx.doi.org/10.4314/njtd.v21i1.2133

Using carbon sources as reducing agent in place of hydrides, the reduction of ilmenite or ferrotitanium alloy in a hydrogen formation medium such as the ethanol-water system involving no alkali combines an in-situ hydrogen production, and hydrogen storage via metal oxides reduction. Though, there is a task of identifying whether the reduction is caused by carbon or by some hydrides or hydrogen formed in situ., such system is unique in creating a highly reducing environment as found in the formation of oxyhydrides (Kobayashi *et al*, 2012).

The carbothermal reduction of metal oxides into their metallic form has been known for decades (Karlsson *et al.*, 2018). Carbon is a strong reducing agent. For example, the use of carbonaceous materials such as graphite and CH_4 (C: ZnO molar ratios of 0 to 1) as reducing agents were employed to significantly lower the reduction temperature of ZnO and avoid recombination (Osinga *et al*, 2004; Wieckert and Steinfeld, 2002). Recent studies in this direction have used carbohydrate biomass such as glucose and cellulose as carbon source to cause the reduction of metal oxides and salts partly into their metallic forms under hydrothermal conditions of 250°C with and without NaOH (Zhou *et al*, 2022). Apart from their use as reducing agents for metal oxides, graphene oxide was shown to double the catalytic hydrogen production of ZnO/ZnS using sacrificial reagents that show a trend of efficiencies as follows: ethanol > methanol > isopropanol > ethylene glycol (Gultom *et al*, 2019).

In this study, the reduction of rutile-ilmenite mineral in an ethanol-water system at 120°C was found to transform the morphologies of the mineral into nanofibers which are hydrogen-rich hydrides that may find application as hydrogen storage materials. Based on EDX results before and after hydrothermal process, the reduction was seen to affect mainly the iron oxides and also aluminosilicates (or Al_2O_3 and SiO_2) in the original mineral. The dominant effect of reduction on ilmenite can be implied from the hydrogen occupation of oxygen vacancies of iron oxides in the formed hydride, η-$Ti_2FeO_{0.2}H_{2.8}$.

II. MATERIALS AND METHODS

A. Materials

The SYSTEC vertical autoclave (model: VB-40), with vessel material made of stainless steel 1.4571 (AISI 316 Ti) was used for the hydrothermal process. It has (autoclave) chamber dimensions (Ø × depth: 344 × 450 mm), chamber volume: 40 L, and external (autoclave) dimensions of W × H × D: 500 × 920 × 740 mm. The autoclave's maximum temperature and pressure are 140°C and 4.0 bar respectively. Rutile-ilmenite ore was obtained from Tafawa Balewa Local Government, Bauchi State, Nigeria. Analytical grade chemicals (Sigma-Aldrich) were used.

B. Carbo-hydrothermal Process

Graphene oxide nanomaterial was prepared from zinc-carbon electrodes of used batteries using electrochemical exfoliation method and was purified to obtain the dried powder (Mohammed *et al.*, 2023). A priori, size reduction and sieving of the rutile-ilmenite ore was carried out to obtain ≤50 μm and ≤100 μm particles and possible phase changes were investigated by its calcination at temperatures of 500, 600, 700, and 800°C. For the hydrothermal process, precisely 10 g of the ore (≤50 μm particles) was mixed with 100 mL of deionized water and 25 mL of graphene suspension (2 mg/mL). The mixture was sonicated for about 15 min, and the resulting solution was separated by centrifugation. The wet composite was dispersed in 200 mL of a deionized water/ethanol mixture (1:1 v/v), placed in the autoclave reactor and thermally treated at 120°C for 4 h. The precipitate was allowed to cool to room temperature. The resulting powdered mixture was filtered, washed with deionized water several times, and dried at 60°C for 2 h.

C. Characterizations

Graphene oxide powder was characterized by transmission electron microscopy (TEM), Energy dispersive X-ray (EDX) spectroscopy and X-ray diffraction (XRD). X-ray fluorescence (XRF) analysis of the rutile-ilmenite mineral was carried out. The mineral and its hydrothermal product were characterized using high-resolution scanning electron microscopy (HRSEM/EDX) and X-ray diffraction (XRD). The single crystal XRD patterns were acquired at room temperature (25°C) and scanning from 8° to 80° at a step of 0.034° using Cu Kα radiation wavelength of 1.5406 Å.

III. RESULTS AND DISCUSSION

A. Structure and Composition of Graphene Oxide

Table 1 shows that the graphene oxide powder used in the hydrothermal process has EDX atomic % composition of C (87.52), O (11.7), Si (0.11) and Cl (0.66), and has C/O atoms ratio of 7.48. There were trace amounts of silicon and chlorine in the graphene oxide powder which were introduced from carbon electrodes and the synthesis procedure. As quartz should contain nearly fifty percent by weight each of Si and O, the relatively high 11.7 wt% of O in the EDX indicates that some of the as-prepared graphene sheets were oxidized. Quartz-based constituents may not be responsible for hydride formation because earlier studies of hydrothermal (200°C) treatment of rutile-quartz concentrate in NaOH solution had noticed no hydride formation (Zanaveskin *et al.*, 2014).

The EDX spectrum in Figure 1(a) supports the elemental compositions provided in Table 1. In addition, the SEM in Figure 1(b) and the acquired TEM images in Figure 2 showed that the graphene oxide is multi-layered with several layers of nanosheets.

Table 1: EDX elemental composition of graphene oxide used

Element	C	O	Si	Cl	Total
Wt%	83.09	14.8	0.25	1.86	100
Atomic %	87.52	11.7	0.11	0.66	100

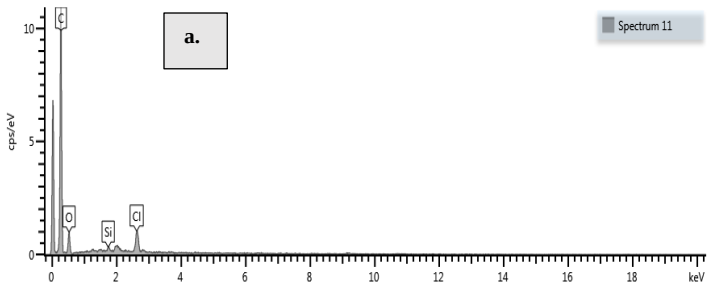

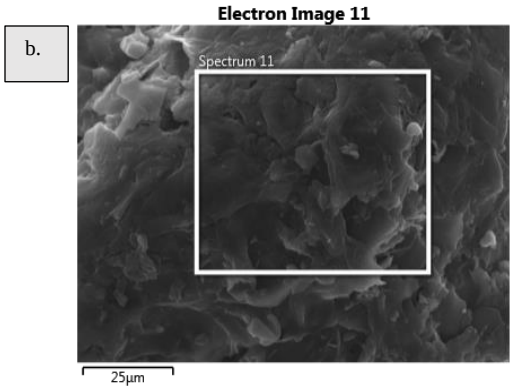

Figure 1: (a) EDX spectrum of graphene oxide, and the (b) corresponding SEM image

The X-ray diffractogram in Figure 3 was also used to confirm the graphene nanosheet (200). It also showed the possible presence of graphite particles (002). Natural graphite/graphite flake possesses a (002) diffraction peak at 26.6°, i.e., d-interlayer spacing distance: ~0.334 nm. After the exfoliation process, the (002) peak gradually shifts from 26.6° to a smaller scattering angle, indicating the presence of graphene nanosheets (Hsieh and Hsueh, 2016). XRD analysis shows the structural changes of graphitic structure which is related to the interplanar expansion. The XRD spectrum of graphite has four intensive peaks. These peaks are at 12.9º (001) plane, 26.5º (002) plane, 42.4º (100) plane and 54.3º (004) plane. Graphite's characteristic peak is one sharp and intensive peak at 26.5º as (002) basal plane. In graphene, this peak becomes broad. Other peaks at 42.4º, 54.3º which

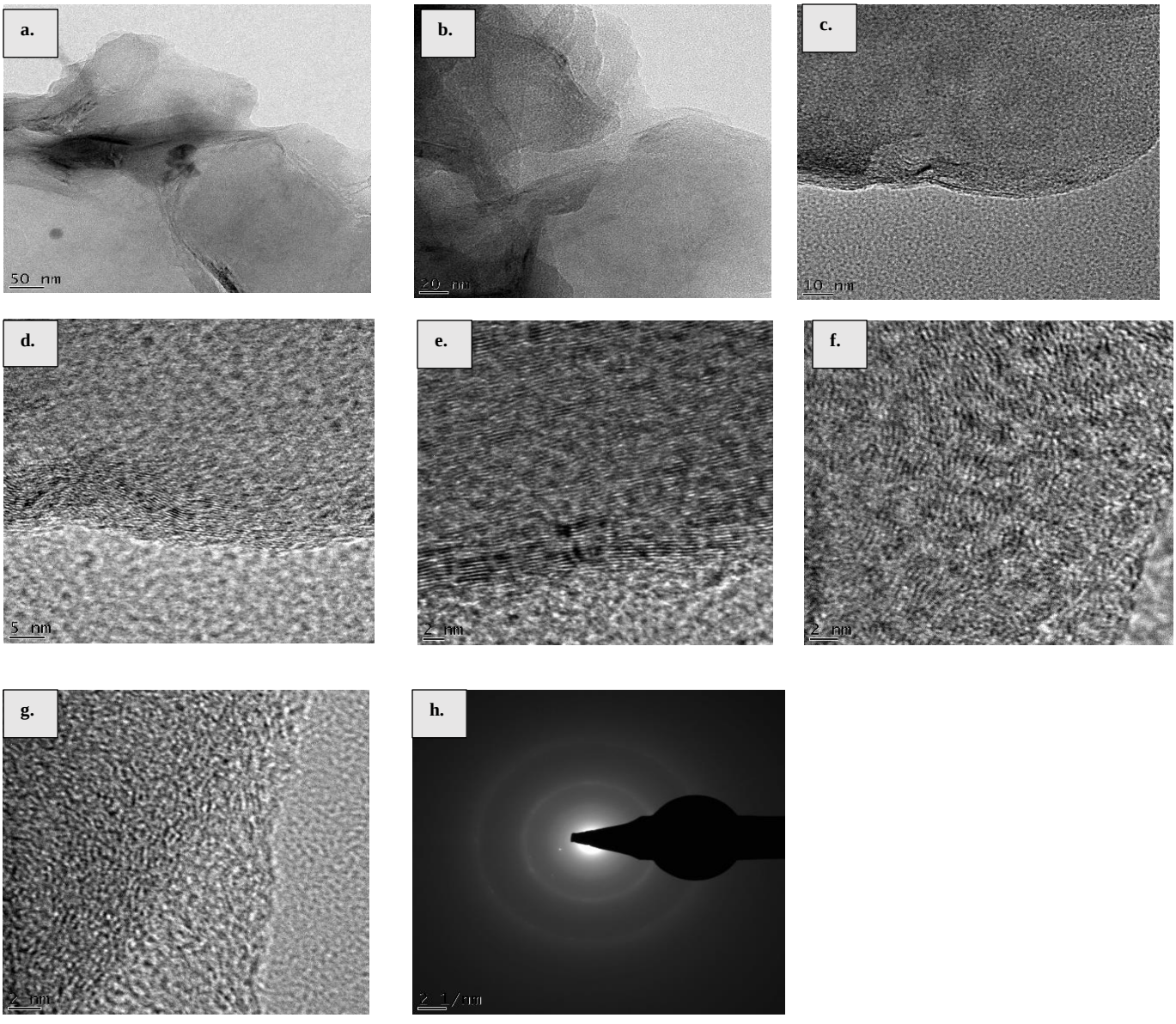

Figure 2: The TEM images of graphene oxide used in carbo-hydrothermal reduction showing (a-c) sheets at 50 nm, 20 nm, and 10 nm magnifications, (d, e) evidence of multilayers, (f, g) lattice fringes, and (h) the SAED pattern.

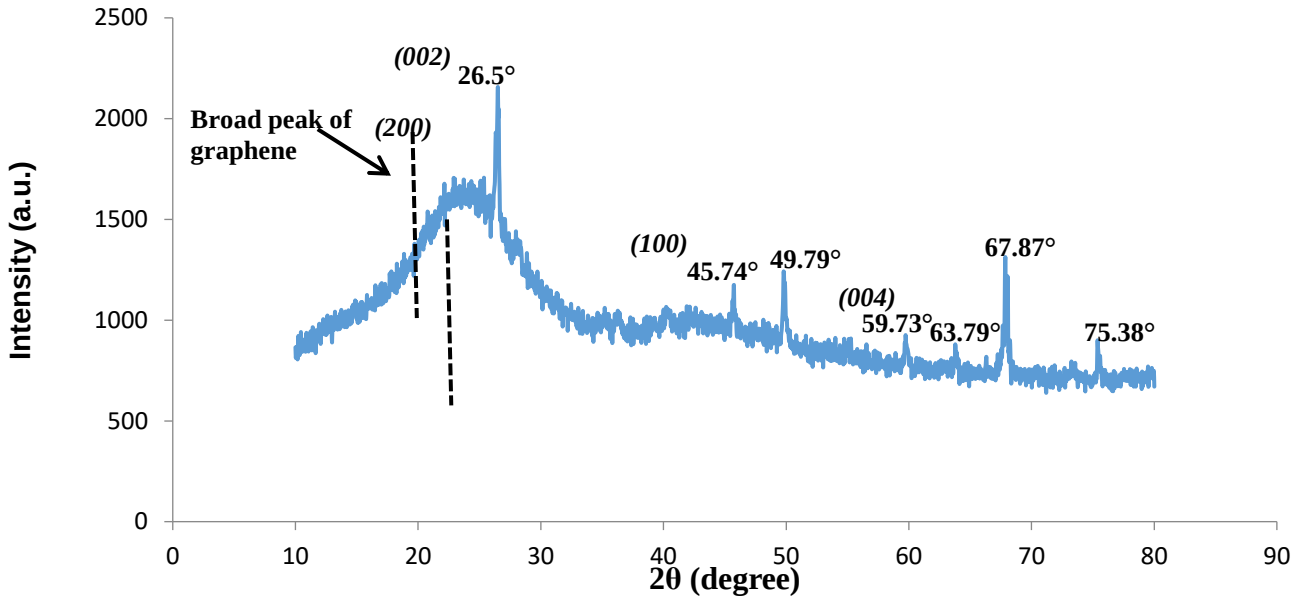

Figure 3: XRD of graphene oxide nanopowder showing evidence of graphene nanosheets with the presence of graphite.

correspond to (100) and (004) crystal planes indicate an increase in interlayer spacing in graphitic structures. These peaks can give ideas about the presence of graphene.

Therefore, XRD analysis confirms the formation of graphene nanosheets. In the diffractogram, the graphitic (002) plane, and the two peaks at (100) and (004) planes are due to graphene. Other peaks are identified as quartz (SiO_2).

B. Rutile-ilmenite Ore and its Response to Thermal Annealing

The composition of rutile-rich ilmenite ore used in the study was determined by X-ray fluorescence (XRF). It represents a titanium-rich mixed oxides system ($FeTiO_3/TiO_2$), with the qualitative XRF analysis showing it to contain mainly elements in the order (wt%): Ti(74.76) > Fe(21.42) > Si(3.52) > Al(1.64). Other elements (P (0.35), S (0.88), K (0.36), Ca (0.42), V (0.25), Mn (0.30), Co (0.67), Ni (0.03), Cu (0.02), Zn (0.06), W (0.06), Rb (0.001), Nb (0.18), Mo (0.20), Sn (0.78), and Sb (0.38)) were present in trace amounts. The qualitative XRF analysis of the rutile ore is presented in Figure 4.

As shown in Figure 5, the XRD of the original rutile-ilmenite mineral reveals that it contained both rutile and anatase phases of titania, including ilmenite and quartz phases.

Thermal treatments at 500, 600, 700 or 800°C transformed the anatase phases of the original ore into rutile phases. However, neither the original rutile-ilmenite ore nor its thermal annealed products in air furnace contain or form hydrides. As shown in Figures 6-8, XRD of the thermally treated rutile mineral revealed that it remained as rutile and ilmenite phases up to 800°C with no obvious influence of particle sizes on their thermal behaviour within 500-800°C temperature that was studied. The only peak differences can be attributed to variations in quartz contents of the samples.

The absence of anatase phases in the thermally treated minerals at 500°C, 600°C, 700°C, and 800°C, which shows that anatase was transformed into the rutile phases is supported by the fact that anatase transforms irreversibly to rutile at elevated temperatures (Hanaor and Sorrell, 2011).

Accordingly, this transformation did not occur during carbo-hydrothermal treatment in the ethanol-water system at the lower temperature of 120°C for 4 hrs. Anatase phases in the original mineral were retained in the reduced product that was obtained after the hydrothermal process. This is supported by the X-ray diffractograms shown in Figure 9 in the next section.

C. Carbo-hydrothermal Formation of $FeTi_2O_{0.2}H_{2.8}$

The *in-situ* generation of hydrogen with simultaneous reduction of rutile-ilmenite ore into its ferrotitanium hydride, η-$FeTi_2O_{0.2}H_{2.8}$ was confirmed using XRD, SEM and SEM-EDX. As revealed in the diffraction patterns of rutile-ilmenite mineral and its reduced form containing graphene oxide given in Figures 9(a) and 9(b), dominant peaks of anatase/rutile titania were obvious. One notes that the peak shift toward lower 2θ (degree) position i.e., higher *d*-spacing (Figure 9a), could be due to the increase in strain and lattice distortion by hydrogen incorporation into the ferrotitanium alloy.

In Figure 9(a), XRD patterns exhibited strong diffraction peaks at 32°, 36° and 54° indicating TiO_2 in the rutile phase. All peaks are in good agreement with the standard spectrum (JCPDS no.: 88-1175 and 84-1286). In the XRD of both the original mineral, and reduced products of the hydrothermal process, characteristics peak due to the distinct phases of rutile (TiO_2), ilmenite ($FeTiO_3$), anatase (TiO_2), and quartz-SiO_2 (or carbon-graphite) are identifiable. XRD of the reduced product contains a new phase, the η-phase $Ti_2FeO_{0.2}H_{2.8}$, in addition to the phases due to rutile, anatase, ilmenite and carbon/graphite which were present in the starting mineral. This is an oxyhydride of $FeTi_2O_x$ (ferropseudobrookite) which was not found in the initial mixture. Equivalent products i.e., hydride of $Ti_4Fe_2O_x$, η-phase hydride $Zr_4Fe_2O_{0.6}H_{5.4}$, and $BaTiO_{3-x}H_x$, possessing cubic Ti_2Ni structure had been reported (Eklöf-Österberg *et al*, 2018; Fjellvåg *et al*, 2019; Stioui *et al*, 1981). The formation of this new, hydrogenated phase from $FeTi_2O_3$ confirms that hydridation occurred during the hydrothermal process. Though the actual crystal lattice structure of

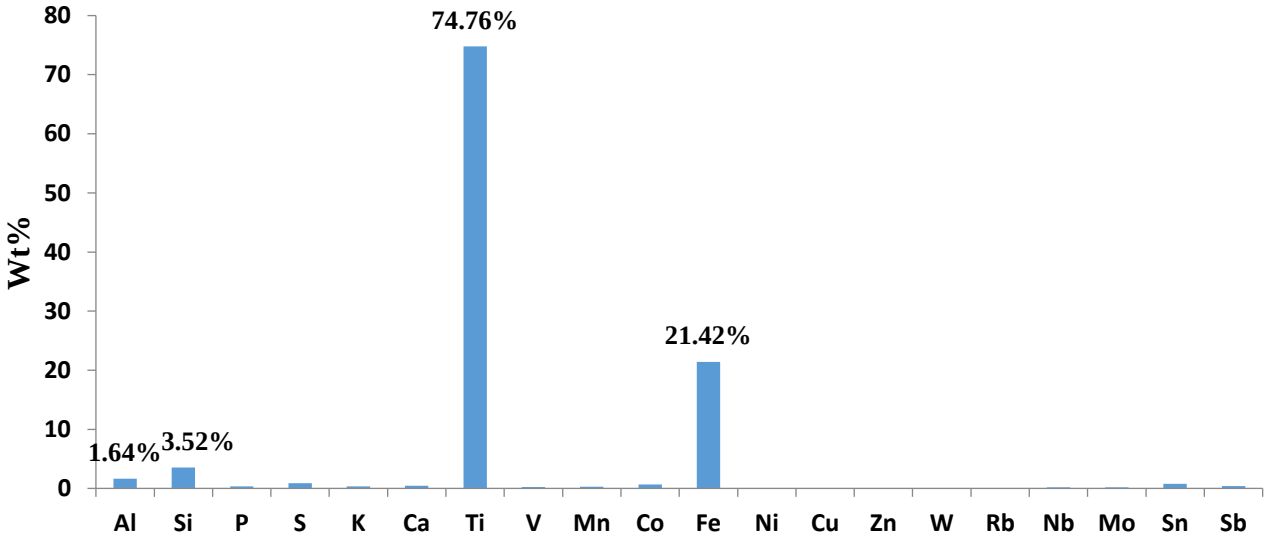

Figure 4. XRF wt% elemental composition of rutile ore

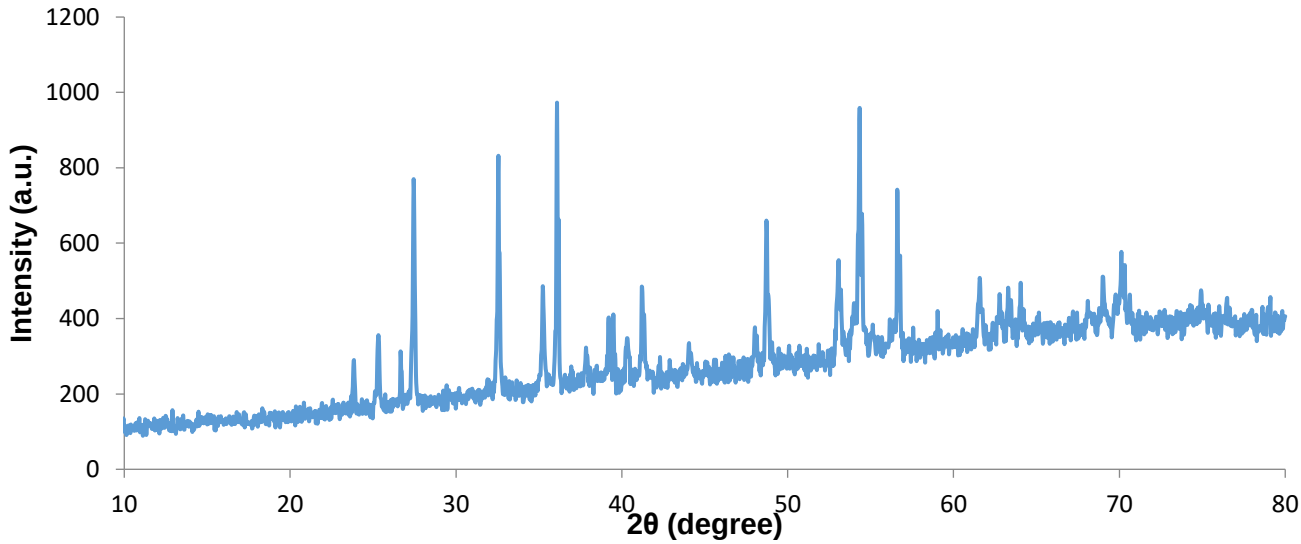

Figure 5: X-ray powder diffraction patterns of original rutile-ilmenite mineral.

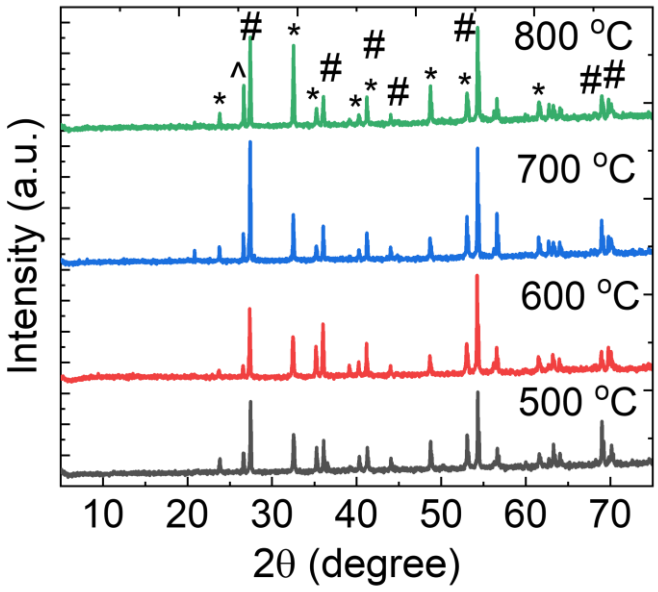

Figure 6: Effects of heat treatment on mesh sub-50 µm rutile-ilmenite mineral particles in air furnace, showing ilmenite (*), quartz (^), and rutile (#) phases.

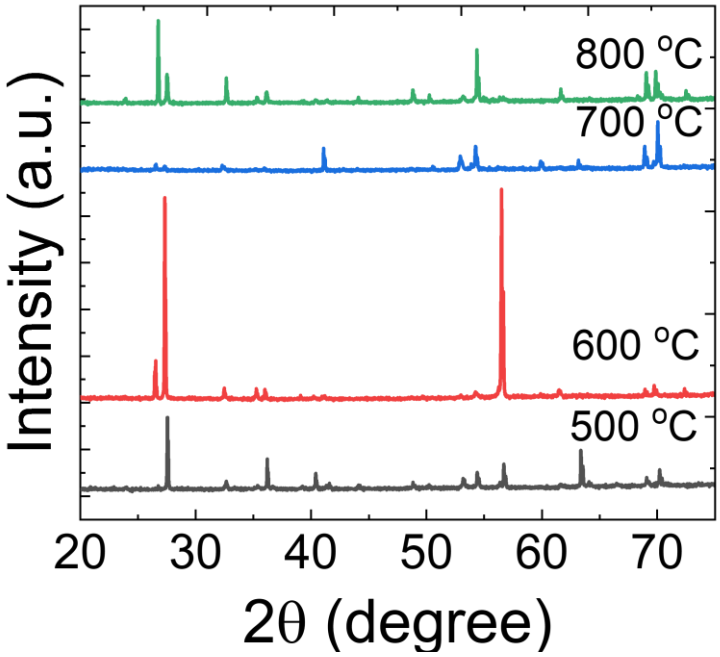

Figure 7: Effects of heat treatment on mesh sub-100 µm rutile mineral particles in air furnace.

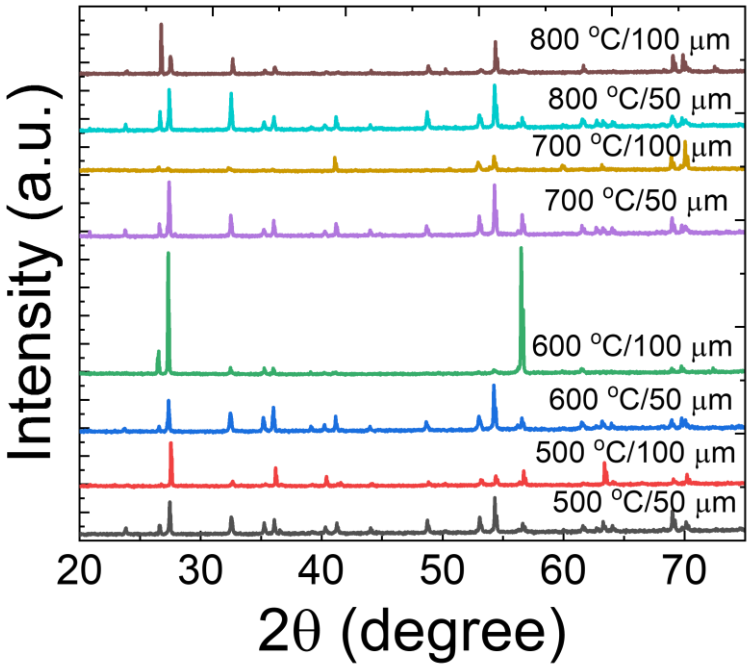

Figure 8: Comparing the phases of thermal annealed rutile-ilmenite ore with 50 µm and 100 µm particle sizes.

$Ti_2FeO_{0.2}H_{2.8}$ is not yet resolved, its strongest peak intensity was at a *d*-spacing of 2.28 Å, and its lattice constant of 9.12 Å is close to that found in $FeTi_2O_3$.

This structure is certainly different from that obtained by Yang *et al.*, (2003). It has been shown in similar compounds that lattice structure is preserved on hydrogenation (Stioui *et al*, 1988). The oxygen-stabilized compound has 2.2 atomic % of oxygen, and it is believed that the iron atom is coordinating, surrounded by oxygen and hydrogen atoms (Aubertin *et al*, 1984).

The phases of rutile type titania (JCPDS#00-021-1276), ilmenite, $FeTiO_3$ (JCPDS#00-029-0733), anatase type titania (JCPDS#00-021-1272), quartz-SiO_2, and carbon-graphite (*JCPDS #00-026-1076*) were confirmed in Figure 10. In the original mineral, the intense peak at 2theta = 26.6° is that of quartz (SiO_2), and in the hydrothermal product, it is due to graphene (graphitic carbon) and maybe new carbonaceous materials deposited from reactions.

In the ICDD database, the new oxyhydride was referenced to a material defined with the compound name, 'iron titanium oxide hydride' (JCPDS#00-036-1385). It was represented in the database by the chemical formula: $Ti_2FeO_{0.2}H_{2.8}$ and empirical formula: $FeH_{2.8}O_{0.2}Ti_2$. The compound's eta (η) phase-modified state could have regular platelet morphology

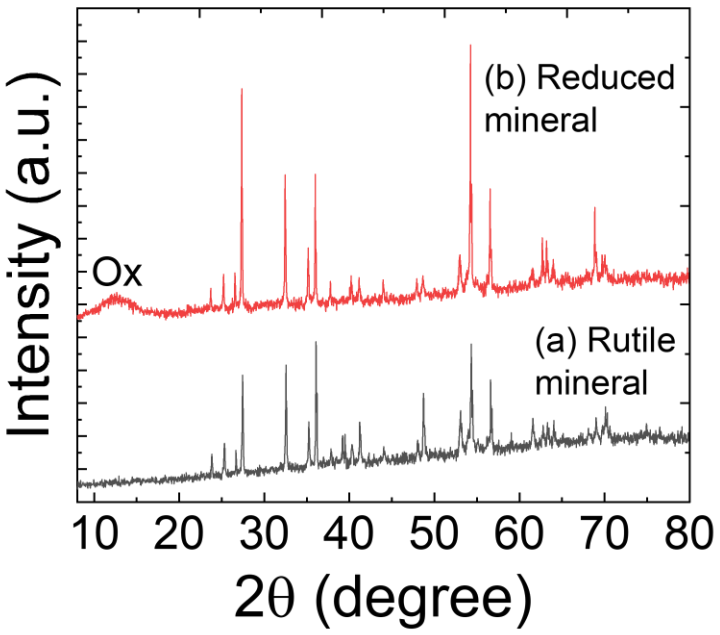

Figure 9: (a) XRD Showing evidence of the formation of amorphous η-phase $Ti_2FeO_{0.2}H_{2.8}$ oxyhydride (b) original mineral.

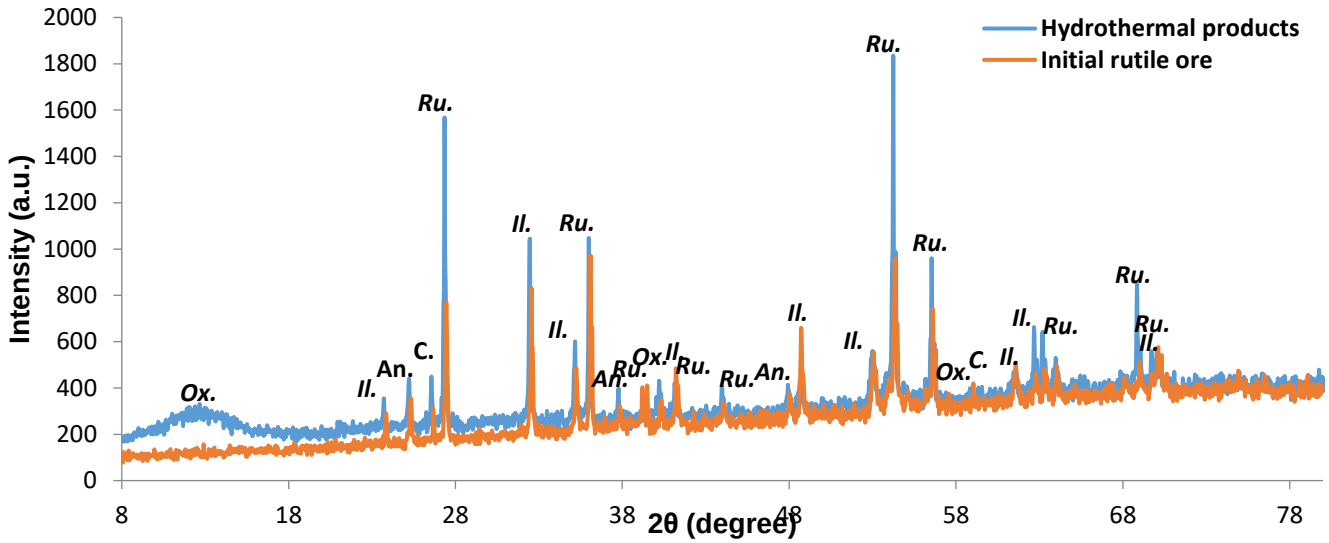

Figure 10: X-ray diffraction pattern of rutile ore and the hydrothermal products (*Ru.* – rutile; *Il.* – ilmenite; *An.* – anatase; *Ox.* – $FeTi_2O_{0.2}H_{2.8}$ oxyhydride; *C.* – carbon. Note: carbon (graphitic) or quartz can diffract at 2-theta peak of 26.6°)

Long *et al.*, (2009). In Figures 11(a-d) and 12(a-d), a comparison of the HRSEM images of the mineral with its hydrothermally reduced product as obtained in the present study shows that the only additional features present in the hydrothermal product were the ≤ 200 nm sized tubular and fibrous structures and some sheets. These are supposed to be the new oxyhydride phase which was also distinctly identified in the XRD pattern.

Based on the reaction conditions involved, the X-ray diffraction, and the structural features in the HRSEM images, a few reaction schemes may be proposed in the formation of η-$Ti_2FeO_{0.2}H_{2.8}$. One possible mechanism is the leaching of ilmenite ($FeTiO_3$) in acidic media, which could take place around 80–150°C in the formation of rutile in autoclaves at atmospheric pressure (Habashi, 2016; Janssen *et al*, 2010). In this scheme, the reductive dissolution of ilmenite occurs when (organic) anions adsorbed at the surface weaken the Fe^{3+}–O bonds, along the zones of weakness in the original ilmenite crystal or an intricate branching network of fractures in the ilmenite (Janssen *et al*, 2010; Schwertmann, 1991). Structural alteration begins at the crystal surface by initial enrichment in ^{18}O isotope. Fracturing may have been driven by volume changes associated with the dissolution of ilmenite and simultaneous reprecipitation of the product phases from an interfacial solution. The rutile inherits crystallographic information from the parent ilmenite, a highly porous product is formed, the original morphology of ilmenite is preserved, and significant depletion in Fe and relative enrichment of Ti could be observed (Janssen *et al*, 2010). The reduction of the highly insoluble iron (III) oxides into the soluble iron (II)

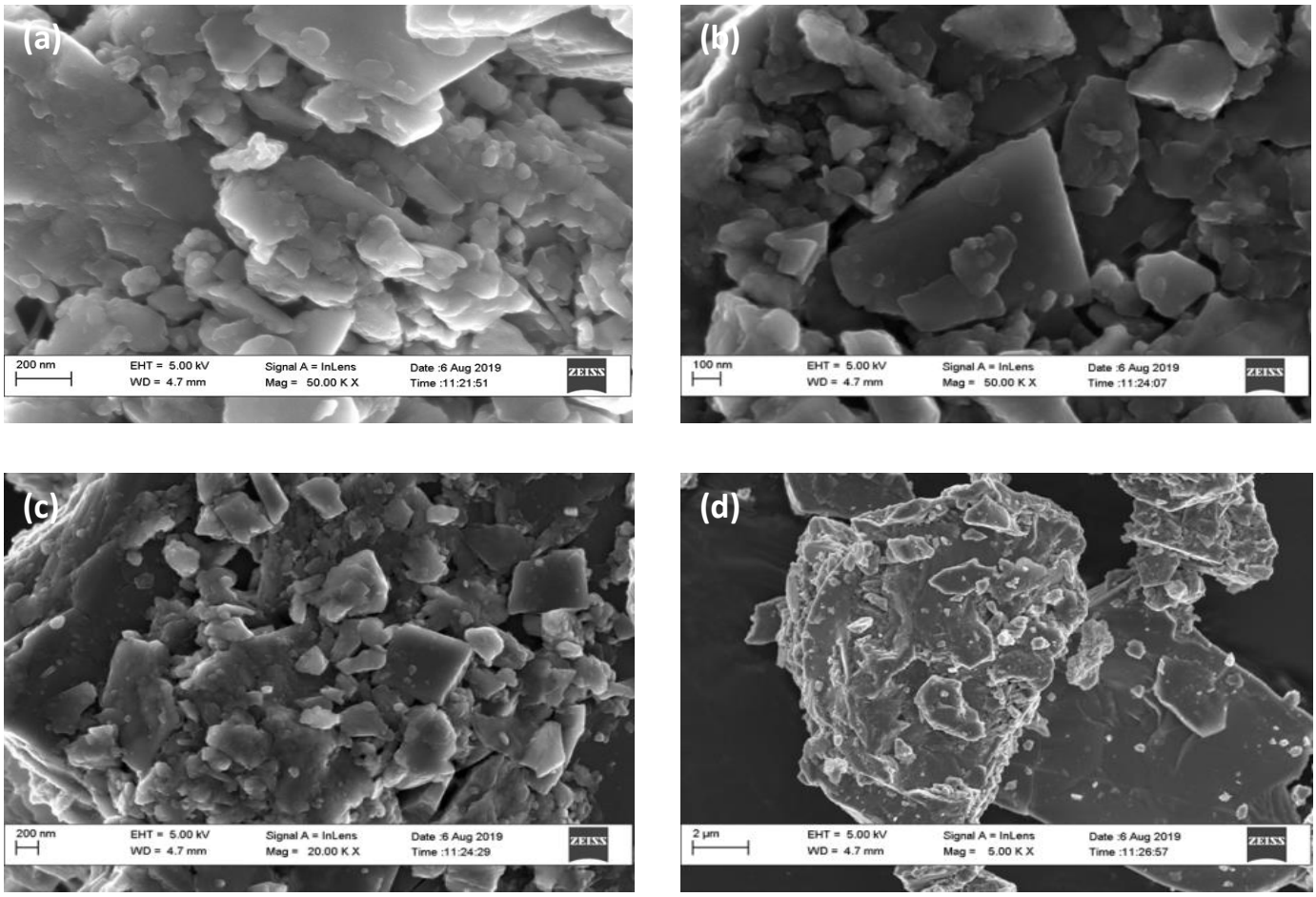

Figure 11(a-d): HRSEM images of the rutile-ilmenite mineral before carbo-hydrothermal treatment. ***Scale bar and magnification:*** **(a) 200 nm/50,000, (b) 100 nm/50,000, (c) 200 nm/20,000, (d) 2 µm/5,000.**

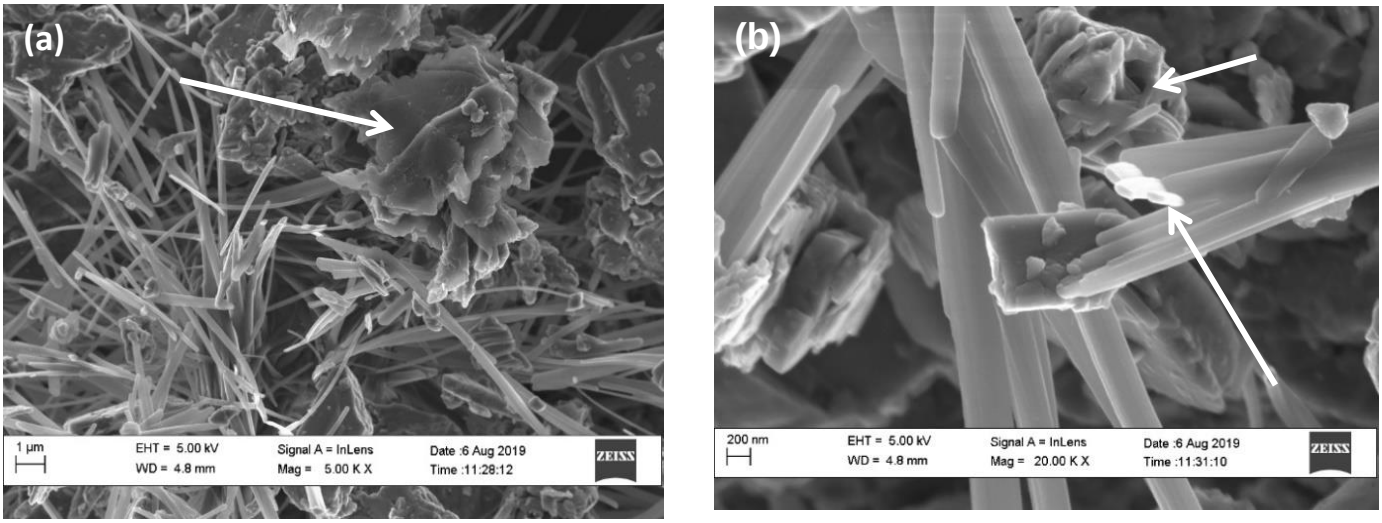

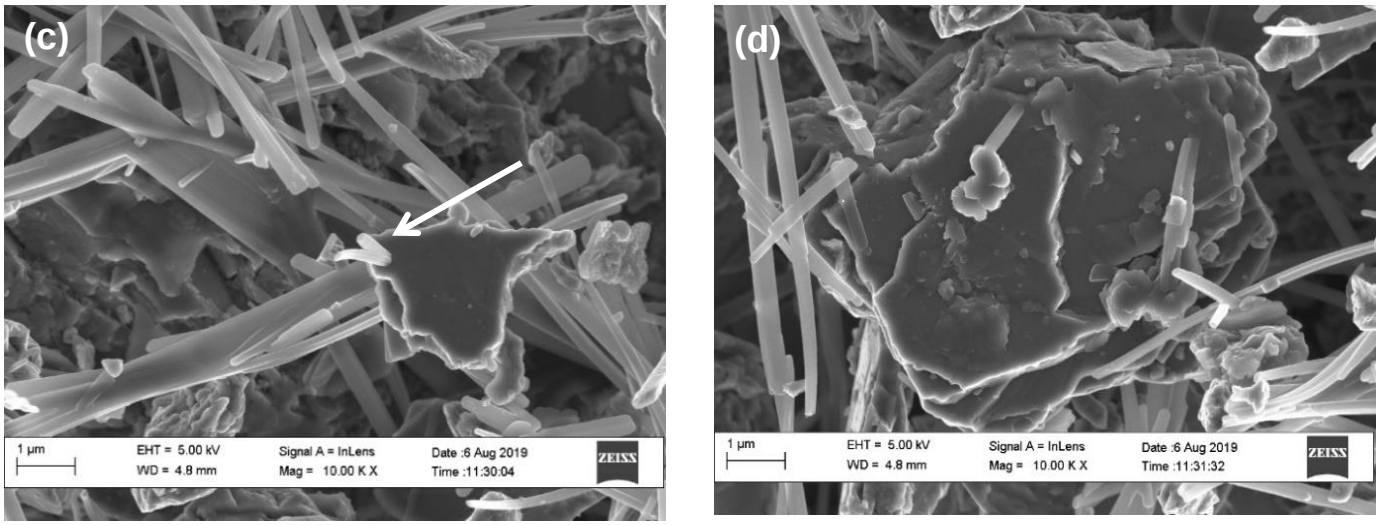

Figure 12: HRSEM images of carbo-hydrothermal product showing evidence of (a) exfoiled sheets of oxide(s) of ilmenite/TiO_2; (b) tubular and fibrous η-$Ti_2FeO_{0.2}H_{2.8}$ structure; and (c), (d) initiation of tubular/fibrous η-$Ti_2FeO_{0.2}H_{2.8}$ growth from bulk oxide(s). *Scale bar and magnification:* (a) 1 µm/5,000, (b) 200 nm/20,000, (c) 1 µm/10,000, (d) 1 µm/10,000.

oxides could occur in the ethanol-water system, a weak acid medium. By this or another reducing system, Eqns. 1(a, b), hydrogen is introduced in the structure.

Oxyhydride formation by reduction:

$$FeTi_2O_3 + xH^- \rightarrow FeTi_2O_{3-x}H_x + \frac{x}{2}O_2 \quad (1a)$$

$$Fe_2Ti_4O_6 + 2xH^- \rightarrow Fe_2Ti_4O_{6-2x}H_{2x} + xO_2 \quad (1b)$$

Another possible mechanism involves the formation of metal hydride i.e., TiH_2 from the metal-steam reaction at the solid-vapor interface with exfoiled anatase TiO_2, and/or reaction between anatase and ethanol, Eqns. (2a, b). The mechanism of exfoiled anatase from the bulk was proposed in the formation of titanate nanotubes (Nakahira *et al*, 2010). This is followed by the reaction between ilmenite ($FeTiO_3$) and the metal hydride (TiH_2) to form ferropseudobrrokite ($FeTi_2O_3$), Eqns. (3a, b). The formation of ferropseudobrookite from ilmenite was due to the inter-diffusion/interaction of (organic) anions with ilmenite-rutile-anatase system. Then, there occurs the reduction of $FeTi_2O_3$ with H_2 from metal hydride into $FeTi_2O_{3-x}H_x$ in which Fe has an oxidation state of II or I (Kim *et al*, 2020), according to Eqns. (2a, b).

Metal hydride formation:

Anatase-steam: $Ti^{4+}O_2^{2-} + 2H^+ \rightarrow Ti^{2+}H_2^- + \frac{3}{2}O_2$ (2a)

Anatase-ethanol: $Ti^{4+}O_2^{2-} + 2C_2H_5OH \rightarrow Ti^{2+}H_2^- + C_4H_{10} + O_2^{2-}$ (2b)

Formation of metastable $FeTi_2O_{0.2}$ (an oxygen-deficient compound) Ferropseudobrookite formation:

$$Fe^{3+}Ti^{3+}O_3^{2-} + Ti^{2+}H_2^- \rightarrow Fe^{2+}Ti_2^{2+}O_3^{2-} + O_2 \quad (3a)$$

$$FeTiO_3 + TiO_2 \rightarrow FeTi_2O_3 + O_2 \quad (3b)$$

The hydride $FeTi_2O_{0.2}H_{2.8}$ has higher hydrogenation capacity compared to the deuteride $Ti_4Fe_2OD_{2.25}$ which has its 16c site completely occupied by oxygen (Zavaliy *et al*, 2007). A hypothetical structure of the oxyhydride $FeTi_2O_{0.2}H_{2.8}$ with Fe as the central coordinating atom would show a hydrogen-to-oxygen atomic ratio of 1: 12, which is equivalent to H/O ratio of 0.23: 2.77 as found in the empirical formula of the oxyhydride.

In addition, there may be carbon deposits due to reactions from ethanol or similar species. In Eqn. (2a), the volume changes caused by inter-diffusion/interaction of steam with the solid rutile-ilmenite-anatase system permitted the formation of TiH_2, and then Eqn. (3a) ferropseudobrookite ($FeTi_2O_3$), which was then reduced into $FeTi_2O_{3-x}H_x$. Ferropseudobrookite could be stable up to 1068°C, and its equilibrium with metallic iron always contains trivalent titanium (Simons and Woermann, 1978). The reduction in Eqn. (3a) can take place, forming a compound such as $FeTi_2O_{3-x}$, in which Fe has an oxidation state of II or I (Kim *et al*, 2020). The ease of hydride formation by $Ti_4M_2O_x$, where (M = Fe, Co, Ni; $0 \leq x \leq 1$), e.g., $Ti_4Fe_2O_x$ has been reported (Aubertin *et al*, 1984).

Such structures - $Zr_4Fe_2O_x$ and $Ti_4Fe_2O_x$ ($0.38 \leq x \leq 1$) need at least 6 atomic% oxygen to stabilize the structure. Stioui *et al* (1988) found that deuterium occupied three different sites in $Ti_4Fe_2OD_{2.25}$. Also, in $FeTi_2O_{0.2}H_{2.8}$, the hydrogen and oxygen share the same lattice site and the ferrous centers in the original paramagnetic ilmenite coordinate the complex. If the path of hydrogen absorption/uptake by the oxides was involved, catalytic materials (such as oxidized graphene) may cause the ethanol steam reforming at the temperature condition to make hydrogen available according to Eqns. 4(a)-(d) (Casas-Ledón *et al*, 2012);

Overall:

$$C_2H_5OH + 3H_2O \rightarrow 2CO_2 + 6H_2 \quad (4a)$$

The catalytic hydrogen generation would involve the simultaneous occurrence or successive stages of reactions:

Ethanol decomposition:

$$C_2H_5OH \rightarrow CO + CH_4 + H_2 \quad (4b)$$

Methane steam reforming:

$$CH_4 + H_2O \rightarrow CO + 3H_2 \quad (4c)$$

Ethanol steam reforming:

$$C_2H_5OH + H_2O \rightarrow CO_2 + CH_4 + 2H_2 \quad (4d)$$

The reduction of the rutile-ilmenite mineral into its hydride can be seen to affect mostly the ilmenite and possibly the Al_2O_3/SiO_2. The reduced form of the powder after carbo-hydrothermal treatment appeared brownish as an indicator of

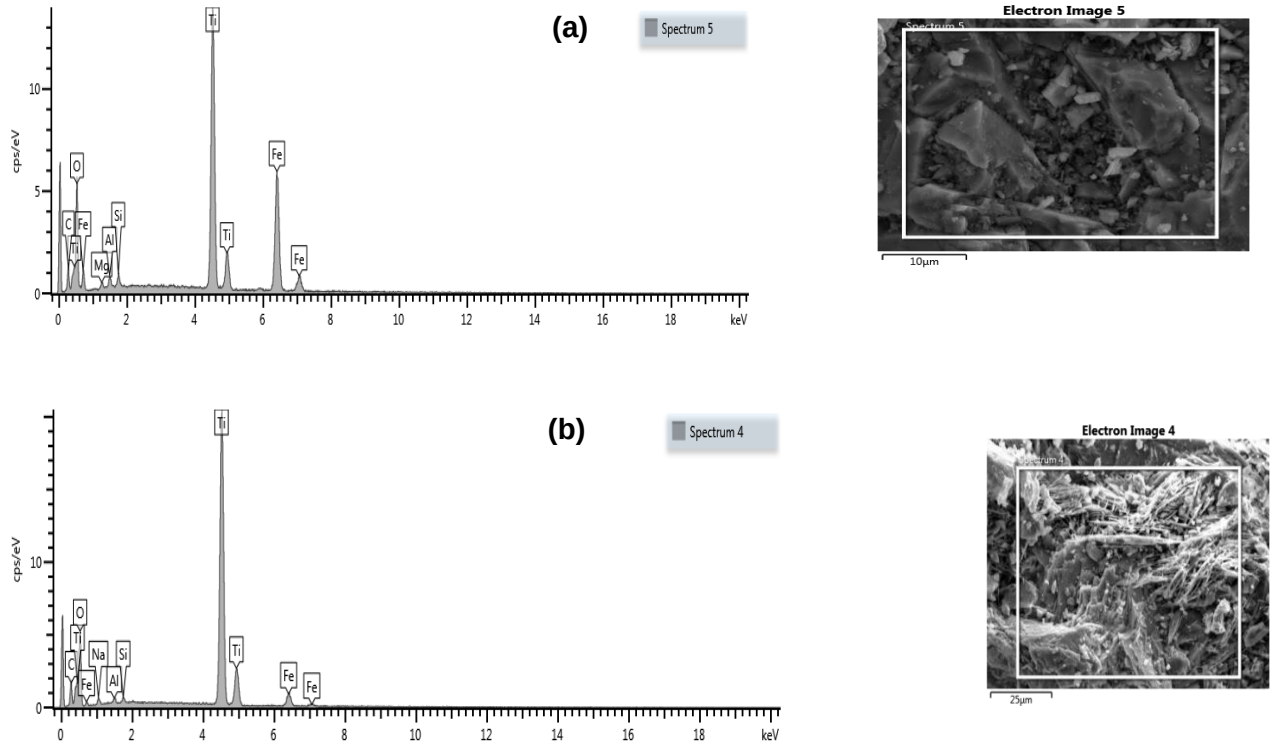

Figure 13: SEM-EDX of (a) original rutile ore, (b) reduced ore from carbo-hydrothermal process.

Table 2: Elemental composition comparison of original rutile-ilmenite with the reduced product

Element	C	O	Mg	Al	Si	Ti	Fe	Total
Before (Wt%)	-	30.24	0.55	0.74	0.73	36.23	31.5	100
After (Wt%)	7.85	36.41	0.94	0.41	0.36	49.55	4.46	100

reduction of ilmenite composition of the original ore. The SEM-EDX result of the original rutile ore and that of the reduced ore obtained from the carbo-hydrothermal treatment is shown in Figure 13. From the EDX result, a reduction in wt% of Fe, Al, Si, and O indicates that the oxides of iron and aluminosilicate in the original mineral were reduced in part or wholly into hydrides or metallic forms. It should be noted that carbon in EDX spectrum of the original ore could be due to carbon coater used during SEM-EDX sample preparation as it was not detected in the EDX composition (as shown in Table 2). A comparison of the oxygen-stabilized Ti-containing hydrides obtained in this study to those of some previous studies is presented in Table 3.

Table 3: Oxygen-stabilized Ti-containing hydrides

S/No	Ti-containing Fe hydrides	Reference
1	η-phase $Ti_2FeO_{0.2}H_{2.8}$	Present study
2	$Ti_2FeO_{0.2}H_{2.6}$	(Wiesinger and Hilscher, 1991)
3	$Ti_4Fe_2OD_{2.25}$	(Stioui *et al*, 1988)
4	$Ti_4Ni_2(O,N,C)D_x$	(Takeshita *et al*, 2002)
5	η-phase $Ti_3ZrNi_2O_{0.5}D_{5.7}$	(Zavaliy *et al*, 2007)

IV. CONCLUSION

The hydrothermic process involving a low-temperature (120°C) reduction of rutile-ilmenite mineral in an ethanol-water medium produced a ferrotitanium oxyhydride which may be useful for hydrogen storage. An oxyhydride $FeTi_2O_{0.2}H_{2.8}$ conforming to the formula $FeTi_2O_{3-x}H_x$ with a likely high hydrogen content in the interstitials was obtained as a reduced form of the original mineral. Formation of the ferrotitanium hydride suggests that hydrogen may be generated from an ethanol-water system at 120°C using the graphene oxide/rutile-ilmenite composite as a catalyst system. Otherwise, a highly reducing environment could be responsible for the formation of the oxyhydride.

ACKNOWLEDGEMENTS

The authors wish to acknowledge the Department of Chemical Engineering, University of Ilorin, Nigeria, for permitting the use of laboratory facilities.

AUTHOR CONTRIBUTIONS

I. A. Mohammed: Conceptualization, Visualization, Methodology. Writing - original draft. **S. I. Mustapha:** Resources, Supervision and Methodology. Validation; **F. A. Aderibigbe:** Resources, Supervision and Methodology. **H. U. Hambali:** Formal analysis, Methodology, Validation; **A. M. Afolabi:** Methodology, Investigation, Validation; **K. B. Muritala:** Methodology, Investigation, Validation; **U. M. Aliyu:** Methodology, Visualization, Validation.

REFERENCES

Aubertin, F.; U. Gonser and S. Campbell. (1984). Hydride formation by zirconium-iron alloys and by η-phase Zr4Fe2O0. 6. Journal of Physics F: Metal Physics, *14*(9): 2213.

Casas-Ledón, Y.; L. E. Arteaga-Perez; M. C. Morales-Perez and L. M. Peralta-Suárez. (2012). Thermodynamic analysis of the hydrogen production from ethanol: first and second laws approaches. International Scholarly Research Notices, *2012*.

Eklöf-Österberg, C.; R. Nedumkandathil; U. Häussermann; A. Jaworski; A. J. Pell; M. Tyagi; N. H. Jalarvo; B. Frick; A. Faraone and M. Karlsson. (2018). Dynamics of hydride ions in metal hydride-reduced BaTiO3 samples investigated with quasielastic neutron scattering. The Journal of Physical Chemistry C, *123*(4): 2019-2030.

Fjellvåg, Ø. S.; V. Øygarden; M. H. Sørby and A. O. Sjåstad. (2019). Crystal structure of LaSr3Fe3O9 and its phase relation with LaSr3Fe3O10. Journal of solid state chemistry, *275*: 56-62.

Gultom, N. S.; H. Abdullah and D.-H. Kuo. (2019). Effects of graphene oxide and sacrificial reagent for highly efficient hydrogen production with the costless Zn (O, S) photocatalyst. International Journal of Hydrogen Energy, *44*(56): 29516-29528.

Habashi, F. (2016). Ilmenite for pigment and metal production. Interdisciplinary Journal of Chemistry, *1*(1): 28-33.

Hanaor, D. A. and Sorrell, C. C. (2011). Review of the anatase to rutile phase transformation. Journal of Materials science, *46*(4): 855-874.

Hsieh, C.-T. and Hsueh, J.-H. (2016). Electrochemical exfoliation of graphene sheets from a natural graphite flask in the presence of sulfate ions at different temperatures. RSC Advances, *6*(69): 64826-64831.

Janssen, A.; A. Putnis; T. Geisler and C. Putnis. (2010). The experimental replacement of ilmenite by rutile in HCl solutions. Mineralogical Magazine, *74*(4): 633-644.

Karlsson, T.; C. Forsgren and B.-M. Steenari. (2018). Recovery of antimony: a laboratory study on the thermal decomposition and carbothermal reduction of Sb (III), Bi (III), Zn (II) oxides, and antimony compounds from metal oxide varistors. Journal of Sustainable Metallurgy, *4*(2): 194-204.

Kim, S. Y.; S. Saqlain; B. J. Cha; S. Zhao; H. O. Seo and Y. D. Kim. (2020). Annealing temperature-dependent effects of Fe-Loading on the visible light-driven photocatalytic activity of rutile TiO2 nanoparticles and their applicability for air purification. Catalysts, *10*(7): 739.

Kobayashi, Y.; O. J. Hernandez; T. Sakaguchi; T. Yajima; T. Roisnel; Y. Tsujimoto; M. Morita; Y. Noda; Y. Mogami and A. Kitada. (2012). An oxyhydride of BaTiO3 exhibiting hydride exchange and electronic conductivity. Nature materials, *11*(6): 507-511.

Long, F.; Y. Yoo; C. Jo; S. M. Seo; H. Jeong; Y. Song; T. Jin and Z. Hu. (2009). Phase transformation of η and σ phases in an experimental nickel-based superalloy. Journal of alloys and compounds, *478*(1-2): 181-187.

Ma, M.; D. Wang; X. Hu; X. Jin and G. Z. Chen. (2006). A direct electrochemical route from ilmenite to hydrogen-storage ferrotitanium alloys. Chemistry–A European Journal, *12*(19): 5075-5081.

Mohammed, I.; F. Aderibigbe; S. Mustapha and T. Adewoye. (2023). Desalination using graphene oxide-cellulose composite membrane.

Nakahira, A.; T. Kubo and C. Numako. (2010). Formation mechanism of TiO2-derived titanate nanotubes prepared by the hydrothermal process. Inorganic chemistry, *49*(13): 5845-5852.

Osinga, T.; U. Frommherz; A. Steinfeld and C. Wieckert. (2004). Experimental investigation of the solar carbothermic reduction of ZnO using a two-cavity solar reactor. J. Sol. Energy Eng., *126*(1): 633-637.

Schwertmann, U. (1991). Solubility and dissolution of iron oxides. Plant and soil, *130*(1): 1-25.

Simons, B. and Woermann, E. (1978). Iron titanium oxides in equilibrium with metallic iron. Contributions to Mineralogy and Petrology, *66*(1): 81-89.

Simpraditpan, A.; T. Wirunmongkol; S. Pavasupree and W. Pecharapa. (2013). Simple hydrothermal preparation of nanofibers from a natural ilmenite mineral. Ceramics International, *39*(3): 2497-2502.

Stioui, C.; D. Fruchart; A. Rouault; R. Fruchart; E. Roudaut and J. Rebiere. (1981). Absorption d'hydrogene par Ti4Fe2O et diverses phases M6O. Materials Research Bulletin, *16*(7): 869-876.

Stioui, M.; A. Resnik; M. Reshotko; A. Grayevsky; D. Shaltiel; N. Kaplan and B. Rupp. (1988). Nuclear magnetic resonance and magnetization studies in Ti4Fe2O0. 4Hx. Journal of the Less Common Metals, *141*(2): 177-190.

Taguchi, K.; K. Shinozaki; H. Okumura; C. Michioka; K. Yoshimura and K. N. Ishihara. (2020). Discovery of Amorphous Iron Hydrides via Novel Quiescent Reaction in Aqueous Solution. Scientific Reports, *10*(1): 1-9.

Takeshita, H. T.; H. Tanaka; T. Kiyobayashi; N. Takeichi and N. Kuriyama. (2002). Hydrogenation characteristics of Ti2Ni and Ti4Ni2X (X= O, N, C). Journal of alloys and compounds, *330*: 517-521.

Wieckert, C. and Steinfeld, A. (2002). Solar thermal reduction of ZnO using CH 4: ZnO and C: ZnO molar ratios less than 1. J. Sol. Energy Eng., *124*(1): 55-62.

Wiesinger, G. and Hilscher, G. (1991). Chapter 6 Magnetism of hydrides *Handbook of Magnetic Materials* (Vol. 6, pp. 511-584): Elsevier.

Yang, J.; Z.Jin; X. Wang; W. Li; J. Zhang; S. Zhang; X. Guo and Z. Zhang. (2003). Study on composition, structure and formation process of nanotube Na 2 Ti 2 O 4 (OH) 2. Dalton Transactions(20): 3898-3901.

Zanaveskin, K.; R. Lukashev; M. Makhin and L. Zanaveskin. (2014). Hydrothermal preparation of porous materials from a rutile–quartz concentrate. Ceramics International, *40*(10): 16577-16580.

Zavaliy, I.; R. Cerny; A. Riabov and I. Saldan. (2007). Crystal structure of the eta-Ti 3 ZrNi 2 O 0.5 suboxide and its Ti 3 ZrNi 2 O 0.5 D 5.7 deuteride. Moscow University Chemistry Bulletin, *48*(1): 187-193.

Zhou, D.; D. Li; S. Yuan and Z. Chen. (2022). Recent Advances in Biomass-Based Photocatalytic H2 Production and Efficient Photocatalysts: A Review. Energy & Fuels, *36*(18): 10721-10731.